Dynamical transition induced by large bubbles in two-dimensional foam flows

I. Cantat* and R. Delannay
GMCM, UMR 6626, Université de Rennes (CNRS), 263 Avenue du Général Leclerc, 35042 Rennes Cedex, France
(Received 12 July 2002; published 13 March 2003)

We study the dynamical behavior of a large bubble embedded in the plug flow of an ordered two-dimensional foam. At a critical velocity, the foam structure becomes instable and the large bubble migrates through the foam faster than the mean flow. This size segregation is due to viscous effects and happens only for flow velocities larger than a given threshold. We present analytical and numerical predictions for the pressure field, the velocity threshold, and the relative velocity of the large bubble. We show that the phenomenon can induce flow destabilization with dramatic effects on foam transport.

DOI: 10.1103/PhysRevE.67.031501 PACS number(s): 83.50.Ha, 82.70.Rr, 83.60.La

Foams are important industrial materials. Their flows exhibit complex behavior involving elastic, plastic, and viscous effects. So far, their rheology has defied attempts to derive general constitutive relations. Since they can be more easily observed and modeled, the flows of two-dimensional (2D) foams have stimulated experimental and theoretical interest [1–6]. A monodisperse foam subject to a pressure gradient in a Hele Shaw cell with smooth lateral boundaries gives rise to a simple plug flow. In contrast, in case of a polydisperse foam, the plug flow undergoes a sharp dynamical transition at a critical velocity threshold v_t. Larger bubbles insinuate themselves through the foam faster than the mean flow, as shown by Lordereau's experiments [7]. Once fully developed, this instability induces strong spatial pressure fluctuations leading to films breakage. It may have dramatic consequences for foam flows in fracture, as encountered in enhanced oil recovery. This phenomenon cannot be explained with a quasistatic point of view. In fact, unlike shear flows, no external constraint enforces bubble reorganization, and changes in the foam structure are intrinsically related to dissipative processes. A large bubble (LB) gives rise to a smaller local film density and, consequently, to a low effective viscosity averaged on a mesoscopic scale. As for the Saffman Taylor instability, large bubbles migration is driven by viscosity contrast. However, the coupling with the elastoplastic response of the film network leads to subtle specific behaviors. This paper is devoted to the determination of similarity laws for the instability threshold and for the large bubble asymptotic velocity in the case of a single large bubble embedded in an ordered foam. We establish analytical expressions for the pressure, tension, and viscous forces below the velocity threshold. These results agree well with numerical simulations and account for the experimental observations qualitatively.

We consider a dry soap froth organized as a monolayer between two horizontal glass plates. The froth experiences a steady push through the cell by newly produced bubbles. Inertial terms are negligible and the force balance on each film involves surface tension, gas pressure, and viscous forces. In a monodisperse regular foam, plug flow occurs without bubble deformation and the viscous force is thus identical for each bubble. As discussed later, this force is related to the friction between the films and depends on the flow velocity. It is balanced by a uniform pressure gap δP between two successive bubbles in the flow direction (Fig. 1). Creating a large bubble by the removal of films suppresses pressure jumps. In order to balance the macroscopic pressure gradient imposed on the foam, such removal must be compensated by larger pressure gaps ΔP_i distributed in a *a priori* unknown way through the adjacent films, as depicted in Fig. 1. As this paper will show, the elastic network distortion adjusts to compensate for this force discrepancy at low velocity, and the plug flow is maintained. Past a critical threshold, the plastic limit is reached and the compensation is driven instead by viscous forces, thus making these films move faster than the mean flow. This qualitative description of the features illustrates the crucial role of dissipative processes being the driving force behind large bubble migration. Their competition with surface tension effects leads to the instability threshold.

The dissipation is localized near the Plateau borders and is associated with fluid viscosity [8]. The no-slip condition imposes large velocity gradients in regions in contact with the glass boundary. Additionally, because the typical bubble size is much larger than the gap between the two plates, these regions of high gradient constitute the major part of the Plateau borders. Consequently, the dissipation is dominated by viscous friction between the film and the plate and thus depends on the local film velocity and not on the velocity dif-

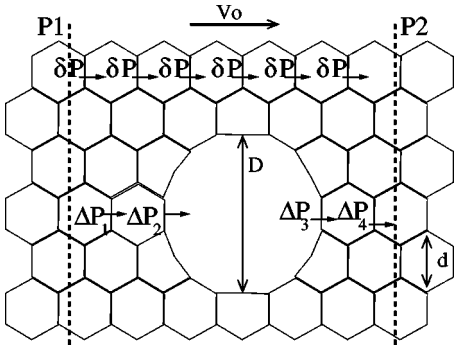

FIG. 1. Schematic view of the pressure field. In order to fulfill the boundary conditions P_1 and P_2, the pressure gaps ΔP_i across films around LB must be larger than the reference δP.

*Email address: isabelle.cantat@univ-rennes1.fr

 ©2003 The American Physical Society

ference between neighboring bubbles. This viscous force may follow various velocity power laws, depending on the local geometry and on the flow rate [9,10]. For the sake of simplicity we assume a linear dependence of the force and a constant overall mobility parameter η, as already proposed in Ref. [3]. This does not affect the qualitative features of our results. The dissipation function is thus $Q=\int \eta v^2\, dl$, where v is the velocity norm of the soap films. The 2D dry foam is described on an overhead view by a line network on which the integral is performed.

At equilibrium, bubble walls are cylindrical, with the curvature in the plane of the glass. In contrast, out of equilibrium films have two nonzero and nonuniform radii of curvature and the very complex resulting shape will be disregarded in our model. Numerically, vertical Plateau borders and bubble walls are represented, respectively, by points at positions r_i (vertices) and by segments l_{ij} connecting these vertices (edges) as done in Ref. [4]. The equations of motion derive from the following energy equation in variational form:

$$\frac{\partial Q}{\partial v_i}+\frac{\partial H}{\partial r_i}=0, \tag{1}$$

where v_i is the velocity of the ith vertex. The dissipation Q is expressed as a discrete sum of contributions from vertex positions

$$Q=\frac{\eta}{2}\sum_{i,j}\frac{l_{ij}}{2}(\mathbf{v}_i)^2, \tag{2}$$

where i varies over all vertices and j represents the three neighbors of vertex i. The energy H is

$$H=\gamma\sum_{i>j} l_{ij}-\sum_k P_k A_k. \tag{3}$$

The first sum is the total interface length, where γ is related to the physical surface tension γ_0 and to the Hele Shaw cell thickness h using $\gamma=2h\gamma_0$. The second term is a sum over all bubbles. The Lagrange multiplier P_k, associated to the kth bubble area A_k, enforces the conservation of the latter. It is related to the physical bubble pressure $P_{0,k}$ by the relation $P_k=hP_{0,k}$ and will be called a pressure. Time scales are too short for gas diffusion to take place, and films do not rupture. This model is the simplest to capture qualitatively the phenomenon of interest.

The numerical simulation is performed in a periodic array and the initial condition is an ordered monodisperse foam of bubbles with uniform size d and a single LB of size D at position $\mathbf{r}_0$. At each time step, a bubble line far from LB is pushed at constant velocity $v_0\mathbf{u}_x$, and other vertices are displaced as prescribed by Eq. (1), which provides an explicit expression for the velocity as a function of the positions. A neighbor swapping event ($T1$ process) is performed when two vertices become closer than a given value ϵd, where ϵ represents the square root of the liquid fraction. After a transient depending on the initial large bubble shape, a stationary regime is reached in which the large bubble exhibits a regular almond shape oriented along the flow (see Fig. 2). Plug flows are observed at low velocity. However, as Fig. 3 illustrates, the large bubble reaches a velocity $v_{LB}>v_0$ for velocities faster than a threshold $v_t\sim\gamma/(\eta D)$.

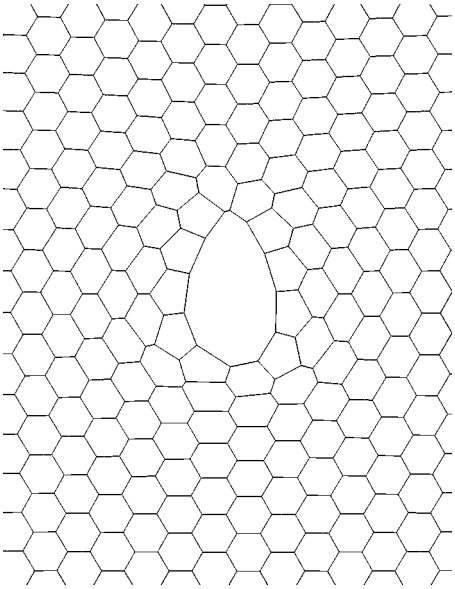

FIG. 2. Large bubble shape in the stationary regime (numerical simulation). The foam flows downwards and $v_0>v_t$. Crystalline organization is recovered behind the large bubble.

It makes its way through two small bubble columns, separating bubbles ahead, and restoring the connections behind. Thus, swapping occurs mainly around two ''fracture points.'' The leading point propagates the fracture and the trailing one heals it. After the transient, the migration of the large bubble does not leave any defect in the foam. However, this simple migration can become more complex in two ways. First, depending on the aspect ratio D/d, a large bubble may carry a few small ones in its wake. Second, it may also entrain dislocations created during the transient. In this case, the initial bubble connections are shifted after the large bubble passes. This behavior creates a rich dynamical phase diagram, which we will analyze further in the future.

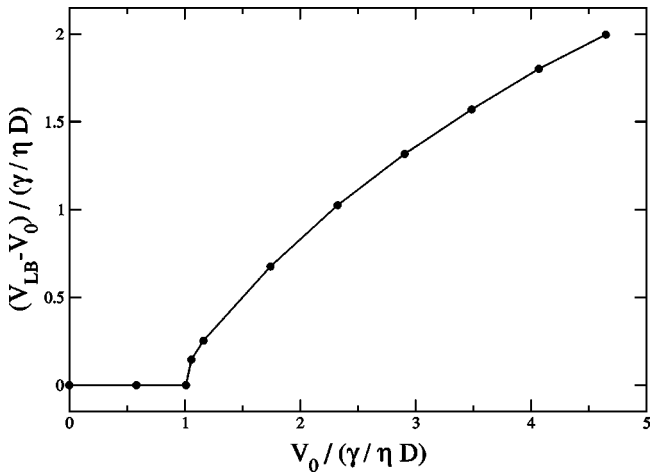

FIG. 3. Large bubble migration velocity. Aspect ratio $D/d=3.5$, $\epsilon=0.1$.

We now develop an analytical prediction of the viscous, tension, and pressure force fields exerted on the foam films below the velocity threshold. From these, we deduce the migration threshold. At equilibrium, the whole pressure field can be determined from a visualization of the film network [11]. Since in a nonquasistatic flow regime, viscous forces induce a finite curvature in planes normal to the transparent plates, it is virtually impossible to infer the pressure difference from images of the flow. Consequently, analytical predictions for the pressure field represent an interesting result by itself.

Below the threshold, all velocities conform to $\mathbf{v}=v_0\mathbf{u}_x$. Outside the large bubble, the total film length is $1/d$ per unit surface of the 2D foam, disregarding a geometrical prefactor close to unity. The viscous force per unit surface, averaged on the scale of a bubble, is thus

$$\mathbf{F}_{visc}=-\frac{\eta v_0}{d}\mathbf{u}_x. \tag{4}$$

The large bubble induces a friction deficit $\delta\mathbf{f}=n\,\eta v_0 d\,\mathbf{u}_x$ proportional to the number n of missing soap films. For $D\gg d$, n is on the order of D^2/d^2. Rearranging Eq. (4) and assuming that the deficit is concentrated at $r=r_0$, we write

$$\mathbf{F}_{visc}=-\nabla\left(\frac{\eta v_0 x}{d}\right)+\delta(\mathbf{r}-\mathbf{r_0})\frac{\eta v_0 D^2}{d}\mathbf{u}_x. \tag{5}$$

For $v_0>v_t$, the large bubble migration modifies the velocity field and induces $T1$ events that increase the dissipation rate.

The spatial distribution of the surface tension stress is more complex. Even at equilibrium the large bubble induces network distortion and inhomogeneities in surface tension stress which are balanced by the equilibrium pressure distribution P_{eq}. This inhomogeneities are intrinsically related to the foam topology: on an average, a bubble is overpressurized if it has less than six neighbors, and underpressurized otherwise [1]. So, in term of resulting equilibrium surface force, the surface tension contribution $\mathbf{F}_{eq}$ counterbalanceds the pressure contribution $-\mathbf{F}_{eq}$. During the flow, in a frustrated attempt to make its way through the foam, the large bubble induces new deformations. Below the threshold, the foam exhibits a linear elastic response. The induced out of equilibrium tension stress is related to the bubble displacement $\mathbf{X}$ from the equilibrium position through an elastic coefficient μ. Since the foam is incompressible, $\boldsymbol{\nabla}\cdot\mathbf{X}=0$ and the elastic surface force is $\mathbf{F}=\mu\nabla^2\mathbf{X}$. Then, the total contribution of the tension to the surface force is

$$\mathbf{F}_{tens}=\mathbf{F}_{eq}+\mu\nabla^2\mathbf{X}, \tag{6}$$

Finally, the pressure forces are decomposed in the same way. We define the dynamical pressure field as $\overline{P}=P-P_{eq}$. Unlike P_{eq}, $\overline{P}$ is smooth even at the bubble scale and its gradient is meaningful, so

$$\mathbf{F}_{press}=-\mathbf{F}_{eq}-\nabla\overline{P}. \tag{7}$$

We combine Eqs. (5)–(7) and find the equation of motion

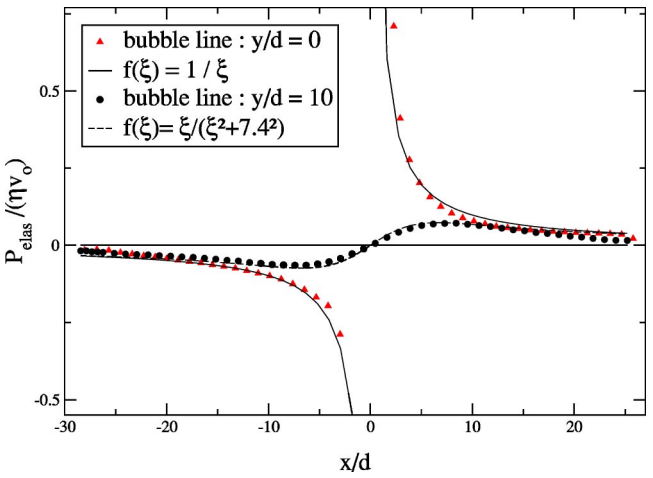

FIG. 4. Pressure for two representative bubble columns oriented along the flow, once P_{eq} and the average pressure gradient have been subtracted, for a velocity ratio $v_0/v_t=0.95$ and an aspect ratio $D/d=3.5$. Symbols are numerical predictions at the positions shown and lines are mathematical functions indicated on the legend. The theory of Eq. (10) predicts a function of similar shape $f(\xi)=1.9\xi/[\xi^2+(y/d)^2]$.

$$-\nabla\left(\frac{\eta v_0 x}{d}+\overline{P}\right)+\mu\nabla^2\mathbf{X}=-\delta(\mathbf{r}-\mathbf{r}_0)\frac{\eta v_0 D^2}{d}\mathbf{u}_x, \tag{8}$$

$$\boldsymbol{\nabla}\cdot\mathbf{X}=0. \tag{9}$$

An analytical solution of these equations exists for a boundless domain (see Ref. [12]), with the asymptotic boundary condition $\eta v_0 x/d+\overline{P}=0$, which corresponds to a vanishing influence of the large bubble at infinity. For our purpose, the determination of the whole displacement field is useless and will be detailed in a future work. The pressure field expression is

$$\overline{P}=-\frac{\eta v_0 x}{d}+\frac{\eta v_0 D^2}{2\pi d}\frac{x-x_0}{(\mathbf{r}-\mathbf{r}_0)^2}, \tag{10}$$

except for the large bubble, for which only the first term applies. Figure 4 compares values of $\overline{P}+(\eta v_0 x/d)$ obtained by the full numerical simulation and the solution of Eq. (10). The theoretical predictions of the latter capture well the functional relationship. Hiding the influence of the large bubble anisotropy, the artificial localization of the missing viscous forces through the distribution δ is presumably responsible for the small scale discrepancies obtained in the y direction (see Fig. 4 and caption). The uncertainty on the prefactor is mainly due to the approximate value of n that can be easily cured at the price of the generality. Finally, the use of periodic conditions for the numerical simulation induces a small overestimation of the dynamical pressure field at a long distance due to the influence of the large bubble periodic images.

The pressure discontinuity at the large bubble boundary is given by the last term in Eqs. (10), with $\mathbf{r}=D/2\mathbf{u}_x$ and must

be counterbalanced by the tension stress. At the migration threshold, this value thus reaches the plastic threshold of the order of γ/d [13] :

$$\frac{\eta v_t D^2}{2\pi d}\frac{2}{D}=\frac{\gamma}{d}. \tag{11}$$

The velocity threshold is thus

$$v_t \sim \frac{\gamma}{\eta D}. \tag{12}$$

For small aspect ratio, the exact value for n in Eq. (5) must be used leading to a diverging threshold for $d=D$. Numerically, the threshold depends linearly on the parameter ϵ governing the $T1$ transformations. An extrapolation at $\epsilon=0$ gives a good agreement with analytical predictions.

For larger velocities, a stationary regime is reached with periodic motion. Elastic energy storage alternates with dissipative $T1$ transformations localized near the large bubble. As the tension forces are limited by the plastic threshold, whereas viscous and pressure forces increase linearly with v_0, it becomes thus negligible in Eq. (9). We get $\overline{P} \sim \eta v_0 x/d$ and the pressure gap on the films at the front and at the rear of the large bubble scales as $\Delta P \sim \eta v_0 D/d$. We deduce the asymptotic velocity law as a function of the different physical parameter:

$$v_{LB} \sim v_0 \frac{D}{d}. \tag{13}$$

The asymptotic behavior is difficult to observe numerically (see Fig. 3). Very large pressure gradients must be imposed on the foam, and the incompressibility constraint becomes hard to ensure. Future experimental investigations will determine if this regime is reached before other mechanisms, such as film ruptures, strongly modify the flow nature.

In conclusion, our study explains the origin of the instability giving rise to the large bubble migration. It predicts the existence of the instability threshold and produces analytical expressions for the corresponding velocity and for the pressure field. A numerical model of an ordered foam agreed well with the predictions. This study naturally leads to new questions on the dynamic interactions between several large bubbles in a bidisperse foam. In particular, we have experimentally observed the formation of long streamwise chains of large bubbles percolating through the Hele Shaw cell. This phenomenon has profound effects on the flow. These chains transport the major part of the volume flux at high speed. The soap films involved are submitted to high stresses, and avalanches of film breakages occur frequently, thus destroying suddenly the whole column and short circuiting the overall pressure drop until a new foam fulfills again the free passage. This process related to the large bubbles interactions and organization is highly undesirable in industrial flow and further studies of this phenomenon are thus of practical interest. The force fields determined in this paper can be easily generalized for sparse large bubbles of various sizes if their effects are additive. An interesting open question is whether a linear elastic coupling generates the interaction observed between large bubbles, or if nonlinear effects dominate. In case of continuous size distribution, we expect very rich dynamical behaviors that remain to be explored.

We are grateful to F. Bolton for his numerical code, which has been the basis for our simulations. We wish to thank C. Caroli, F. Graner, and M. Louge for enlightening discussions.

[1] D. Weaire and S. Hutzler, *The Physics of Foams* (Oxford University press, Oxford, 2000).
[2] A.M. Kraynik and M.G. Hansen, J. Rheol. **31**, 175 (1987).
[3] J.A. Glazier and D. Weaire, J. Phys.: Condens. Matter **4**, 1867 (1992).
[4] T. Okuzono and K. Kawasaki, Phys. Rev. E **51**, 1246 (1995).
[5] S. Tewari *et al.*, Phys. Rev. E **60**, 4385 (2001).
[6] G. Debregeas, H. Tabuteau, and J.-M. diMeglio, Phys. Rev. Lett. **87**, 178305 (2001).
[7] O. Lordereau, Ph.D. thesis, Université de Rennes, 2002.
[8] H.M. Princen, J. Colloid Interface Sci. **118**, 201 (1987).
[9] H. Wong, C.J. Radke, and S. Morris, J. Fluid Mech. **292**, 71 (1995).
[10] F.P. Bretherton, J. Fluid Mech. **10**, 166 (1961).
[11] F. Graner, Y. Jiang, E. Janiaud, and C. Flament, Phys. Rev. E **63**, 011402 (2001).
[12] J. Happel and H. Brenner, *Low Reynolds Number Hydrodynamics* (Martinus Nijhoff, Dordrecht, 1986).
[13] H.M. Princen, J. Colloid Interface Sci. **91**, 160 (1983).